Filtering Power Divider With Ultrawide Stopband and Wideband Low Radiation Loss Using Substrate Integrated Defected Ground Structure

Changxuan Han, *Student Member, IEEE*, Deshan Tang, *Student Member, IEEE*, Zhixian Deng, *Graduate Student Member, IEEE*, Huizhen Jenny Qian, *Member, IEEE*, and Xun Luo, *Senior Member, IEEE*

***Abstract*— In this letter, a novel substrate integrated defected ground structure (SIDGS) resonant cell is proposed. Such SIDGS resonant cells can not only introduce an ultrawide stopband for spurious suppression but also achieve low radiation loss in a wideband, which can be easily implemented in passive circuits with high performance. To verify this mechanism, a filtering power divider (FPD) using the folded stepped-impedance scheme is developed. Here, two coupled SIDGS resonant cells are cascaded at the arms of the power divider to achieve a filtering response with ultrawideband harmonic suppression. The fabricated FPD is operated at 2.87 GHz (i.e., the passband center frequency f_0) with a 3-dB fractional bandwidth (FBW) of 23%, which exhibits the 28-dB attenuation upper stopband with a low radiation loss even up to 25 GHz (i.e., 8.71 f_0).**

***Index Terms*— Filtering power divider (FPD), high isolation, low radiation loss, substrate integrated defected ground structure (SIDGS), ultrawide stopband.**

I. Introduction

With the ever-developing demands of complex microwave circuits and systems, passive components with wideband interference suppression are developed rapidly. As a key component in modern wireless communication systems, the power divider with filtering function and wide stopband has drawn great attention recently. In [1]–[6], the substrate integrated waveguide (SIW) is proposed for the power-divider design with low radiation loss, which suffers from the narrow stopband. To extend the stopband bandwidth, the low-pass filter [7], stepped-impedance resonators (SIR) [8]–[11] and defected ground structure (DGS) [12]–[17] are proposed. However, the stopband performances of these methods are limited by the restriction of fabrication techniques. Recently, slow wave DGS resonators [18], [19] are presented to further enhance the stopband performance. Such resonators can not only allocate the intrinsic fundamental resonance but also introduce an ultrawide stopband with high rejection level. Nevertheless, high radiation makes conventional DGS hard to be integrated in passive circuits. Therefore, the design of filtering power divider (FPD) with ultrawide stopband and low radiation loss for flexible integration still remains great challenges.

Manuscript received September 17, 2020; accepted November 3, 2020. Date of publication November 17, 2020; date of current version February 11, 2021. This work was supported in part by NSFC under Grant 61934001 and Grant 61904025. *(Corresponding author: Xun Luo.)*

The authors are with the Center for Advanced Semiconductor and Integrated Micro-System, UESTC, Chengdu 611731, China (e-mail: xun-luo@ieee.org).

Color versions of one or more figures in this letter are available at https://doi.org/10.1109/LMWC.2020.3036419.

Digital Object Identifier 10.1109/LMWC.2020.3036419

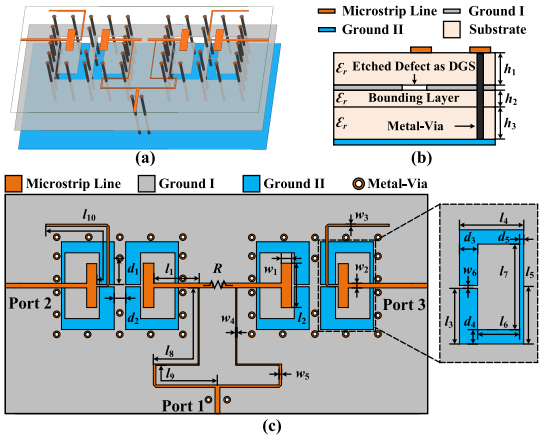

Fig. 1. Configuration of the proposed FPD. (a) 3-D view. (b) Layer diagram. (c) Top view.

In this letter, a novel substrate integrated DGS (SIDGS) resonant cell is proposed. Such an SIDGS resonant cell consists of a DGS resonator integrated between two substrate layers, where a bottom grounded plane and surrounding metal-vias are introduced as an integrated package. The proposed resonant cell can not only reserve the harmonic suppression characteristic of the DGS resonator but can also be easily integrated in passive circuits with low radiation. Based on the proposed SIDGS resonant cell, an FPD with ultrawide stopband and low radiation loss is the design and fabricated.

II. Schematic and Operation

Fig. 1 depicts the configuration of the proposed FPD. Two pairs of coupling SIDGS resonance cells are cascaded on the output arms of a Wilkinson power divider, while the microstrip T-stubs act as feed lines. Note that the etched defect area in the SIDGS resonant cells can be defined as the DGS since the physical dimensions of such a scheme cannot meet the theoretical definitions of slotline [20]. To investigate the characteristics of the FPD, the design tools advanced design system (ADS), CST Microwave Studio, and dielectric substrate Rogers 4003C with resin bounding layer (i.e., $\varepsilon_r = 3.55$, $h_1 = h_3 = 0.203$ mm, and $h_2 = 0.1$ mm) are used.

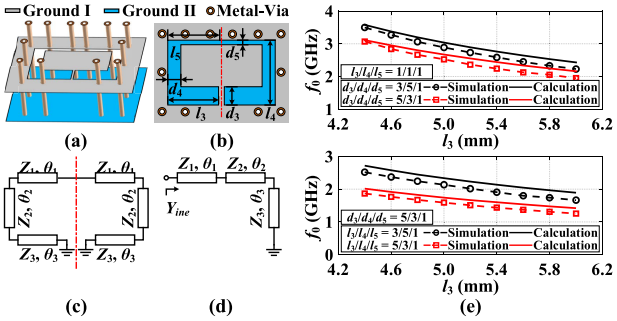

Fig. 2. Configuration of the proposed SIDGS resonant cell. (a) 3-D view. (b) Top view. (c) Simplified equivalent circuit model. (d) Even-mode model. (e) Fundamental resonance of the SIDGS cell versus l_3.

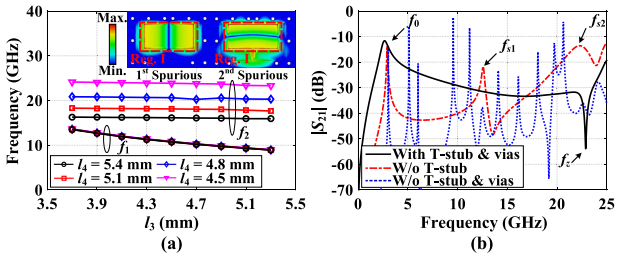

Fig. 3. (a) Electric field distributions of the first and second spurious resonant modes and the two spurious resonant-mode frequencies f_1 and f_2 versus l_3 with various l_4. (b) Simulated frequency responses of the SIDGS resonant cell in different configurations ($l_3 = 3.9$, $l_4 = 4.7$, $l_5 = 4.0$, $d_3 = 1.4$, $d_4 = 1.0$, and $d_5 = 0.3$, unit: mm).

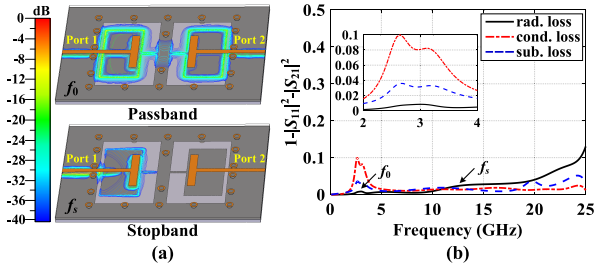

Fig. 4. (a) Electric field distribution of the SIDGS filter at the passband frequency (i.e., $f_0 = 2.9$ GHz) and stopband frequency (i.e., $f_s = 12.7$ GHz). (b) Simulated loss responses of the SIDGS filter (rad.: radiation; cond.: conductor; and sub.: substrate).

A. Substrate Integrated DGS

1) Resonance: The configuration of the proposed SIDGS is shown in Fig. 2(a) and (b). A C-shape etched defect is located on the ground I, which is integrated between two substrate layers. Besides, a bottom grounded plane and surrounding metal-vias are introduced as a package. The etched defect in the SIDGS resonant cell is similar to a $\lambda/2$ SIR with two grounded ends [21], which allocates the intrinsic fundamental resonance. To obtain the fundamental resonant frequency, the simplified equivalent circuit of the SIDGS resonant cell is derived, as shown in Fig. 2(c). It can be seen that the proposed structure is symmetric to the dotted line. Since the symmetric plane at the odd mode is equivalent grounded, the odd-mode resonant frequency exhibits twice the even-mode case (i.e., the symmetric plane at the even mode is equivalent open). Therefore, the fundamental resonance occurs when the even-mode input admittance (i.e., Y_{ine}) is equal to zero, as shown in Fig. 2(d). Y_{ine} can be calculated by (1), as shown at the bottom of the page, where the characteristic impedance and electrical length of the SIDGS can be obtained by the pole-splitting method [22] with full-wave simulations. Then, Fig. 2(e) depicts the effects of physical dimension (i.e., l_3) on the resonant frequency (i.e., f_0) with various ratios of $d_3/d_4/d_5$ and $l_3/l_4/l_5$. Note that the slight deviation between the calculated and simulated results is mainly caused by the influence of the folded structure [23].

2) Stopband Characteristics: Since the etched defect is packaged by the ground II and metal-vias, the TEM spurious resonant modes are introduced at higher frequency [24]. By using the eigenmode solver in the CST Microwave Studio, the spurious resonant modes can be observed in Fig. 3(a). Note that the parallel plate region (i.e., Reg. I) allocates the first and the second TEM mode spurious (i.e., f_{s1} and f_{s2}). Fig. 3(a) illustrates that these spurious resonant-mode frequencies can be adjusted by the physical dimensions l_3 and l_4, respectively. Besides, the frequency responses of the SIDGS resonant cell in different configurations are depicted in Fig. 3(b). It can be seen that most spurious resonances are suppressed by the metal-vias. Meanwhile, the proposed SIDGS could achieve a wide stopband once a microstrip T-stub locates at the symmetric plane as a feed line. In this case, the feed line is placed at the virtual grounding of the first spurious resonant mode; hence, f_{s1} is suppressed. Moreover, a deep transmission zero f_z created by the T-stub can be used to reduce the f_{s2}. Thus, as shown in Fig. 3(b), the SIDGS resonant cell with a microstrip T-stub can achieve an ultrawide stopband.

3) Radiation Loss: The electric and magnetic fields of conventional DGS are distributed in an open space, which leads to large electromagnetic radiation [23]. Such radiation leads to an extra passband insertion loss and electromagnetic interference. To investigate the loss characteristic of the SIDGS, a two-order filter using the proposed SIDGS resonant cell is implemented. The electric field distributions of the filter are shown in Fig. 4(a). Note that the electric fields' contribution of SIDGS is mainly restricted in a quasi-cavity by ground II and metal-vias. With such characteristics, the SIDGS can effectively reduce the radiation loss compared with the conventional DGS [25]. Besides, the proposed SIDGS can be easily integrated into passive circuits design due to the surrounding of a complete ground plane. The loss responses of the filter using the proposed SIDGS are shown in Fig. 3(a). Here, the radiation loss is simulated under the case of lossless metal and substrate (i.e., S_{11r} and S_{21r}). The radiation loss L_r is calculated by

$$L_r = 1 - |S_{11r}|^2 - |S_{21r}|^2. \tag{2}$$

Once the radiation loss is obtained, the conductor loss and substrate loss (i.e., L_c and L_s) can be calculated using (3) under the cases of lossless substrate and lossless metal (i.e.,

$$Y_{\text{ine}} = -j\frac{1}{Z_1}\frac{Z_1Z_2 - Z_1Z_3\tan\theta_2\tan\theta_3 - Z_2Z_3\tan\theta_1\tan\theta_3 - Z_2^2\tan\theta_1\tan\theta_2}{Z_2Z_3\tan\theta_3 + Z_2^2\tan\theta_2 + Z_1Z_2\tan\theta_1 - Z_1Z_3\tan\theta_1\tan\theta_2\tan\theta_3} \tag{1}$$

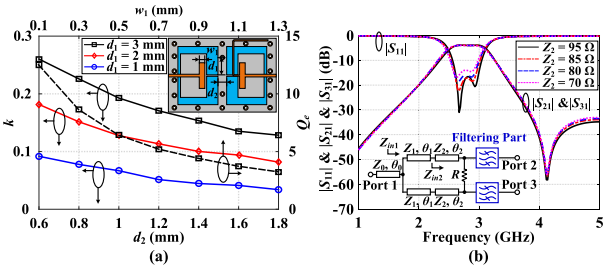

Fig. 5. (a) Configuration of the filtering part and efforts of dimension d_1, d_2, and w_1 on the coupling coefficient k and external Q_e. (b) Schematic of the Wilkinson power divider and simulated $|S_{11}|$, $|S_{21}|$, and $|S_{31}|$ with various Z_2 ($Z_1 = 70.7\ \Omega$, $\theta_1 = 38°$, and $\theta_2 = 58°$ at the center frequency f_0).

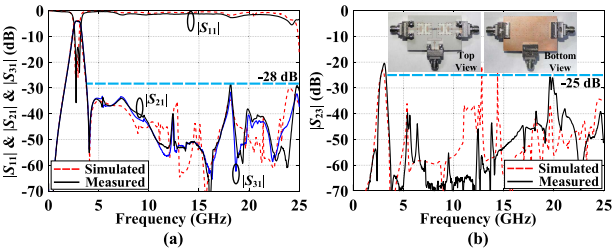

Fig. 6. Measured, simulated results, and the photographs of the proposed FPD ($d_1 = 2.3$, $d_2 = 1.0$, $d_3 = 1.3$, $d_4 = 1.0$, $d_5 = 0.3$, $l_1 = 3.8$, $l_2 = 4$, $l_3 = 3.9$, $l_4 = 4.6$, $l_5 = 4.0$, $l_6 = 2.9$, $l_7 = 6$, $l_8 = 10.9$, $l_9 = 7.2$, $l_{10} = 11.6$, $w_1 = 1.1$, $w_2 = 0.42$, $w_3 = 0.2$, $w_4 = 0.1$, and $w_5 = 0.22$, unit: mm). (a) $|S_{11}|$, $|S_{21}|$, and $|S_{31}|$. (b) $|S_{23}|$.

S_{11c}, S_{21c}, S_{11s}, and S_{21s}), respectively

$$L_{c,s} = 1 - |S_{11c,s}|^2 - |S_{21c,s}|^2 - L_r. \tag{3}$$

It is that the bandpass filter using SIDGS resonant cells exhibits low radiation loss in a wide frequency range. Moreover, the passband insertion loss is mainly contributed by the conduct and substrate losses. Compared with the filter using a microstrip resonator [26], the SIDGS filter exhibits the following advantages.

1) The SIDGS resonant cell with T-stub feed line could introduce a wide stopband, while the microstrip resonator suffers from the harmonic interference.
2) Lower radiation loss is introduced by the SIDGS filter compared with the microstrip type. Thus, the proposed filter is attractive for the integrated circuit with strong electromagnetic compatibility.

B. FPD Design

To verify the aforementioned characteristics, an FPD operating at 2.87 GHz with a 3-dB FBW of 23% is designed based on the SIDGS resonant cell. Such a power divider is composed of two filtering parts and a stepped-impedance Wilkinson power divider. As shown in Fig. 5(a), a pair of SIDGS resonant cells and T-stubs constitute the filtering part. The coupling coefficient k and external quality factor Q_e of the filtering part can be obtained from the desired center frequency f_0 and 3-dB FBW [27]. k can be adjusted by the dimension d_1 and d_2, while the dimension w_1 is the critical element to dominate Q_e. Besides, a $\lambda/4$ open stub is added on T-stub to generate a transmission zero at the upper stopband, which could improve the passband selectivity. Then, the stepped-impedance scheme in Fig. 5(b) is used for the Wilkinson power-divider design to achieve good impedance matching with a compact size. The return loss of port 1 is varied with Z_2, which is optimized once $Z_2 = 95\ \Omega$. The isolated resistor is chosen as 180 Ω to enhance output isolation.

TABLE I
COMPARISON OF STATE-OF-THE-ART FPDS

Ref.	[6]	[7]	[8]	[10]	[19]	**This work**
Tech.*	SIW	Microstrip	Microstrip	Microstrip	DGS	**SIDGS**
f_0 (GHz)	4.82	0.9	2.37	2.02	2.31	**2.87**
IL**	2 dB	1.6 dB	0.3 dB	1 dB	1.2 dB	1 dB
Return Loss	>14 dB	>15 dB	>21.4 dB	>15 dB	>18 dB	**>15 dB**
Stopband Rejection	N/A	>20 dB ($11.1f_0$)	>10 dB ($3.4f_0$)	>40 dB ($4.55f_0$)	>30 dB ($8.66f_0$)	**>28 dB ($8.71f_0$)**
Passband Isolation	N/A	>23 dB	>16 dB	>22 dB	>17 dB	**>20 dB**
Stopband Isolation	N/A	N/A	N/A	>22 dB ($4.41f_0$)	>28 dB ($8.66f_0$)	**>25 dB ($8.71f_0$)**
Radiation Loss	Low	High	High	High	High	**Low**
Size	$0.39\lambda_g^2$	$0.02\lambda_g^2$	$0.17\lambda_g^2$	$0.05\lambda_g^2$	$0.38\lambda_g^2$	**$0.10\lambda_g^2$**

*: Technology. **: Insertion loss.

III. FABRICATION AND MEASUREMENT

Based on the abovementioned principles, an FPD operating at 2.87 GHz with 3-dB FBW of 23% is fabricated. The photograph of the fabricated FPD is shown in Fig. 6. Note that the metal-vias near port 1 are used to ensure that ground I and ground II have the same electrical potential, which can reduce the performance degeneration caused by the SMA connector. The prototype exhibits a compact core-circuit size of 29.8 mm × 14.9 mm (i.e., $0.46\lambda_g \times 0.23\lambda_g$, where λ_g is the microstrip-guided wavelength at 2.87 GHz). The measured results depicted in Fig. 6 are performed using the Agilent N5244A PNA-X network analyzer over the frequency range from 0.01 to 25 GHz. The measured minimal passband insertion loss is 1.1 dB, excluding 3-dB division loss. Meanwhile, the proposed FPD could achieve an ultrawide upper stopband up to 25 GHz (i.e., $8.71\,f_0$) with a rejection level greater than 28 dB. Besides, a transmission zero is created at 4.05 GHz to improve the passband selectivity. The in-band isolation greater than 20 dB is measured. The performance summary and comparison with state-of-the-art FPDs are shown in Table I, which reveals that the proposed FPD shows competitive merits of the insertion loss, stopband performance, isolation, and radiation loss.

IV. CONCLUSION

In this letter, a novel SIDGS resonant cell is proposed for the high-performance integrated system design. Compared with the conventional DGS, such SIDGS can not only introduce a wide stopband performance but also reduce the radiation loss in a wideband. Based on the proposed SIDGS resonant cell, an FPD with low insertion loss, ultrawideband harmonic suppression, and low radiation loss is developed. With such good performances, the proposed FPD using SIDGS is attractive for integrated systems with wideband spurious suppression.

REFERENCES

[1] U. Rosenberg, M. Salehi, J. Bornemann, and E. Mehrshahi, "A novel frequency-selective power combiner/divider in single-layer substrate integrated waveguide technology," *IEEE Microw. Wireless Compon. Lett.*, vol. 23, no. 8, pp. 406–408, Aug. 2013.

[2] Y. M. Huang *et al.*, "Substrate-integrated waveguide power combiner/divider incorporating absorbing material," *IEEE Microw. Wireless Compon. Lett.*, vol. 27, no. 10, pp. 885–887, Oct. 2017.

[3] A. Moulay and T. Djerafi, "Wilkinson power divider with fixed width substrate-integrated waveguide line and a distributed isolation resistance," *IEEE Microw. Wireless Compon. Lett.*, vol. 28, no. 2, pp. 114–116, Feb. 2018.

[4] R. V. Gatti and R. Rossi, "Hermetic broadband 3-dB power divider/combiner in substrate-integrated waveguide (SIW) technology," *IEEE Trans. Microw. Theory Techn.*, vol. 66, no. 6, pp. 3048–3054, Jun. 2018.

[5] Y. Zhou *et al.*, "Slow-wave half-mode substrate integrated waveguide 3-dB Wilkinson power divider/combiner incorporating nonperiodic patterning," *IEEE Microw. Wireless Compon. Lett.*, vol. 28, no. 9, pp. 765–767, Sep. 2018.

[6] X. Wang, X.-W. Zhu, L. Tian, P. Liu, W. Hong, and A. Zhu, "Design and experiment of filtering power divider based on shielded HMSIW/QMSIW technology for 5G wireless applications," *IEEE Access*, vol. 7, pp. 72411–72419, Jun. 2019.

[7] W.-M. Chau, K.-W. Hsu, and W.-H. Tu, "Filter-based Wilkinson power divider," *IEEE Microw. Wireless Compon. Lett.*, vol. 24, no. 4, pp. 239–241, Apr. 2014.

[8] P. Cheong, K.-I. Lai, and K.-W. Tam, "Compact Wilkinson power divider with simultaneous bandpass response and harmonic suppression," in *IEEE MTT-S Int. Microw. Symp. Dig.*, Anaheim, CA, USA, May 2010, pp. 1588–1591.

[9] H. Zhu, A. M. Abbosh, and L. Guo, "Wideband four-way filtering power divider with sharp selectivity and wide stopband using looped coupled-line structures," *IEEE Microw. Wireless Compon. Lett.*, vol. 26, no. 6, pp. 413–415, Jun. 2016.

[10] M.-T. Chen and C.-W. Tang, "Design of the filtering power divider with a wide passband and stopband," *IEEE Microw. Wireless Compon. Lett.*, vol. 28, no. 7, pp. 570–572, Jul. 2018.

[11] P. Wen *et al.*, "Dual-band filtering power divider using dual-resonance resonators with ultrawide stopband and good isolation," *IEEE Microw. Wireless Compon. Lett.*, vol. 29, no. 2, pp. 101–103, Feb. 2019.

[12] D. Ahn, J.-S. Park, C.-S. Kim, J. Kim, Y. Qian, and T. Itoh, "A design of the low-pass filter using the novel microstrip defected ground structure," *IEEE Trans. Microw. Theory Techn.*, vol. 49, no. 1, pp. 86–93, Jan. 2001.

[13] C.-S. Kim, D.-H. Kim, I.-S. Song, K. M. K. H. Leong, T. Itoh, and D. Ahn, "A design of a ring bandpass filters with wide rejection band using DGS and spur-line coupling structures," in *IEEE MTT-S Int. Microw. Symp. Dig.*, Long Beach, CA, USA, Jun. 2005, pp. 2183–2186.

[14] J. Park, J.-P. Kim, and S. Nam, "Design of a novel harmonic-suppressed microstrip low-pass filter," *IEEE Microw. Wireless Compon. Lett.*, vol. 17, no. 6, pp. 424–426, Jun. 2007.

[15] J.-K. Lee and Y.-S. Kim, "Ultra-wideband bandpass filter with improved upper stopband performance using defected ground structure," *IEEE Microw. Wireless Compon. Lett.*, vol. 20, no. 6, pp. 316–318, Jun. 2010.

[16] A. Balalem, A. R. Ali, J. Machac, and A. Omar, "Quasi-elliptic microstrip low-pass filters using an interdigital DGS slot," *IEEE Microw. Wireless Compon. Lett.*, vol. 17, no. 8, pp. 586–588, Aug. 2007.

[17] A. Boutejdar, A. Batmanov, A. Omar, and E. Burte, "A miniature 3.1 GHz microstrip bandpass filter with a suppression of spurious harmonic using multilayer technique and defected ground structure open loop-ring," in *Proc. Ultra-Wideband, Short Pulse Electromagn.* New York, NY, USA: Springer-Verlag, May 2010, pp. 185–191.

[18] X. Luo, J.-G. Ma, E.-P. Li, and K. Ma, "Hybrid microstrip T-stub/defected ground structure cell for electromagnetic interference bandpass filter design," *IEEE Trans. Electromagn. Compat.*, vol. 53, no. 3, pp. 717–725, Aug. 2011.

[19] L. Fan, H. Qian, B. Yang, G. Wang, and X. Luo, "Filtering power divider with wide stopband using open-stub loaded coupled-line and hybrid microstrip T-stub/DGS cell," in *IEEE MTT-S Int. Microw. Symp. Dig.*, Philadelphia, PA, USA, Jun. 2018, pp. 1–4.

[20] R. Garg, I. Bahl, and M. Bozzi, *Microstrip Lines Slotlines*, 3rd ed. Boston, Norwood, MA, USA: Artech House, 2013, p. 246.

[21] X. Luo, J.-G. Ma, and E.-P. Li, "Hybrid microstrip/DGS cell for filter design," *IEEE Microw. Wireless Compon. Lett.*, vol. 21, no. 10, pp. 528–530, Oct. 2011.

[22] J.-S. Hong, *Microstrip Filters for RF/Microwave Applications*, 2nd ed. Hoboken, NJ, USA: Wiley, 2011.

[23] S. V. Robertson and L. P. B. Katehi, "A planar quasi-optical mixer using a folded-slot antenna," *IEEE Trans. Microw. Theory Techn.*, vol. 43, no. 4, pp. 896–898, Apr. 1995.

[24] H. Shigesawa, M. Tsjui, and A. A. Oliner, "Conductor-backed slot line and coplanar waveguide: Dangers and full-wave analyses," in *IEEE MTT-S Int. Microw. Symp. Dig.*, New York, NY, USA, May 1988, pp. 199–202.

[25] Y. Rao, H. J. Qian, B. Yang, R. Gomez-Garcia, and X. Luo, "Dual-band bandpass filter and filtering power divider with ultra-wide upper stopband using hybrid microstrip/DGS dual-resonance cells," *IEEE Access*, vol. 8, pp. 23624–23637, Jan. 2020.

[26] C. Han, Y. Rao, H. J. Qian, and X. Luo, "High-selectivity bandpass filter with wide upper stopband using harmonic suppression structure," in *Proc. IEEE Int. Symp. Radio-Freq. Integr. Technol. (RFIT)*, Nanjing, China, Aug. 2019, pp. 1–3.

[27] X. Luo, B. Yang, and H. J. Qian, "Adaptive synthesis for resonator-coupled filters based on particle swarm optimization," *IEEE Trans. Microw. Theory Techn.*, vol. 67, no. 2, pp. 712–725, Feb. 2019.